

INTERACTION OF LASER RADIATION WITH MATTER https://doi.org/10.1070/QEL16888

Symmetric nanostructuring and plasmonic excitation of gold nanostructures by femtosecond Laguerre–Gaussian laser beams

N.I. Busleev, S.I. Kudryashov, P.A. Danilov, A.P. Porfir'ev, I.N. Saraeva, A.A. Rudenko, S.F. Umanskaya, D.A. Zayarnyi, A.A. Ionin, S.N. Khonina

Abstract. **Femtosecond low-energy Laguerre–Gaussian pulses of tightly focused visible laser radiation were employed for single-pulse ablative nanostructuring of a 50-nm thick gold film. Similar pulses of lower energy were employed for the efficient plasmonic photoluminescence excitation of a rhodamine 6G dye monolayer in the fabricated nanostructures. The consistency between the shape and polarisation symmetries of the low-energy laser beam, on the one hand, and the gold nanostructures produced by the same beam at a high radiation energy, on the other hand, opens the way to consistent nanostructuring and surface-enhanced analytical spectroscopy with the use of nanostructures.**

Keywords: *thin-film nanotexturing, femtosecond laser pulses, Laguerre–Gaussian beams, polarisation states, dye photoluminescence, surface electromagnetic waves.*

1. Introduction

Laser beams with spatially phase- and amplitude-modulated ('structured') wave fronts as well as with different polarisations are a new universal optical tool for modern nanophotonics [1–12]. The laser beam transformation techniques based on this tool may be harnessed not only for a complicated matter structuring with characteristic micrometre or nanomicrometre linear dimensions by subtractive (ablative removal by laser radiation) [5] or translational (capillary surface transfer) [6] procedures, but also for the investigation of preliminarily structured substance [7–9]. These new possibilities have marked a new phase in the investigation of the interaction between structured light and structured substance [4].

Recent years have seen the demonstration of nano- and microtexturing of smooth surfaces with the use of laser beams with spatially modulated intensity profiles [3–5, 10, 11]; the fabrication of chiral surface nano- and microobjects by helical laser beams [1–3, 6]; multiple-pulse self-organisation of radial or azimuthal surface wave-like structures in laser fields with the corresponding polarisations [3, 12], modern surface-enhanced analytical spectroscopy (for instance, Raman scattering enhanced due to the surface structure) of organic compounds with the use of nanostructures and high-order harmonic generation using structured laser beams (for instance, by selecting different types of multipolar Mie resonances in structures [7], including the exotic excitation of the anapole mode [8]). These possibilities for the highly efficient light--substance interaction were provided by matching: (i) the laser wavelength to the size-dependent spectral positions of plasmonic or dielectric Mie resonances; (ii) the intensity profile of the radiation beam and its transverse dimensions to the topology and scale of structured substance; and (iii) the symmetry of the laser field structure to the interacting matter. The study of the possibilities for structuring light and matter to ensure their efficient and controllable coupling in the course of improved laser processing and surface-enhanced analytical spectroscopy with the use of nanostructures is still at its infancy.

In this paper we consider the ablative texturing of a thin gold film by single low-energy femtosecond pulses of tightly focused structured laser radiation and the subsequent dye photoluminescence on the resultant nanostructures efficiently excited by similar pulses at a lower subablative energy.

2. Experimental facility and methods of investigation

A gold 50-nm thick film was produced by magnetron sputtering of 99.99% pure gold target on VK-7 glass plates in the atmosphere of argon at a pressure of 4–5 mbar. The single-pulse surface ablation of the film was carried out with the second harmonic radiation of the pulsed fibre laser Satsuma (Amplitude Systems) with a wavelength of 515 nm, a half-height line width of 1.7 nm, and a pulse duration of 200 fs. The radiation pulses (TEM_{00} mode, $M^2 \approx 1.07$) with energies $\mathcal{E} < 2$ μJ and a pulse repetition rate of 0–2 MHz were delivered to the optical system (Fig. 1) mounted on a vibration-isolated optical table (Standa, Lithuania). The initial linearly

N.I. Busleev, I.N. Saraeva, D.A. Zayarnyi P.N. Lebedev Physical Institute, Russian Academy of Sciences, Leninsky prosp. 53, 119991 Moscow, Russia; S.P. Korolev Samara National Research University, Moskovskoe shosse 34, 443086 Samara, Russia;
e-mail: busleevni@lebedev.ru;
S.I. Kudryashov P.N. Lebedev Physical Institute, Russian Academy of Sciences, Leninsky prosp. 53, 119991 Moscow, Russia; National Research Nuclear University 'MEPhI', Kashirskoe shosse 31, 115409 Moscow, Russia;
P.A. Danilov, A.A. Rudenko, A.A. Ionin P.N. Lebedev Physical Institute, Russian Academy of Sciences, Leninsky prosp. 53, 119991 Moscow, Russia;
A.P. Porfir'ev, S.N. Khonina S.P. Korolev Samara National Research University, Moskovskoe shosse 34, 443086 Samara, Russia; Image Processing Systems Institute, Russian Academy of Sciences – Branch of the Federal Research Centre 'Crystallography and Photonics', Russian Academy of Sciences, Molodogvardeiskaya ul. 151, 443001 Samara, Russia;
S.F. Umanskaya P.N. Lebedev Physical Institute, Russian Academy of Sciences, Leninsky prosp. 53, 119991 Moscow, Russia; National Research Nuclear University 'MEPhI', Kashirskoe shosse 31, 115409 Moscow, Russia; S.P. Korolev Samara National Research University, Moskovskoe sh. 34, 443086 Samara, Russia

Received 25 October 2018; revision received 27 November 2018
Kvantovaya Elektronika **49** (7) 666–671 (2019)
Translated by E.N. Ragozin

polarised Gaussian beam was transformed to azimuthally or radially polarised Laguerre–Gaussian beams using a commercially available S-wave plate (Altechna R&D, Lithuania) (Figs 1 and 2), and the linear polarisation in the Laguerre–Gaussian beam was recovered with the help of $\lambda/4$ plates placed in front of the S-plate or immediately after it.

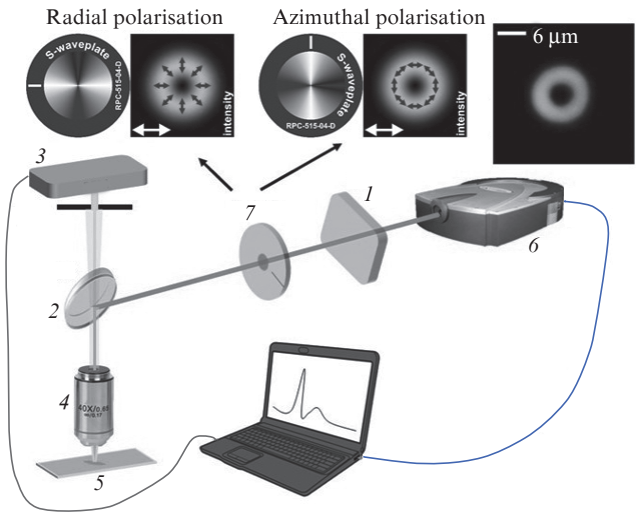

Figure 1. Arrangement of the optical elements for the transformation with an S-wave plate of the profile and polarisation of the laser beam, ablative nanotexturing and photoluminescence excitation in a microscope-spectrophotometer:
(*1*) reflective attenuator; (*2*) beam splitter; (*3*) photomultiplier; (*4*) microscope objective; (*5*) gold film; (*6*) laser; (*7*) S-wave plate; the insets at the top display the corresponding transformations of the initial linear polarisation (indicated with white arrows) of laser radiation for different orientations of the S-wave plate as well as the final profile of the Laguerre–Gaussian beam in the focal plane.

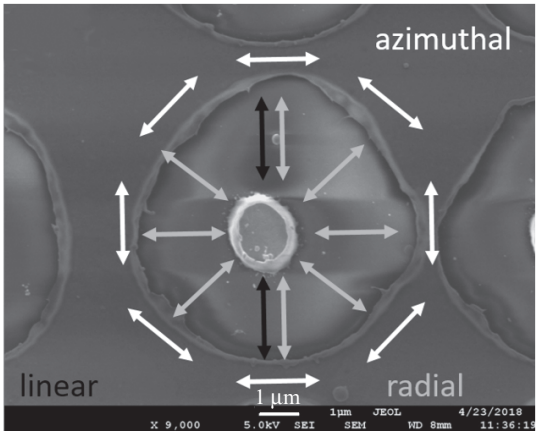

Figure 2. Scheme of the spatial interaction of the Laguerre–Gaussian laser beams with linear (black arrows), radial (grey arrows), and azimuthal (white arrows) polarisations with the structured microhole in the photoluminescence excitation for NA = 0.25.

Next, the laser pulses were fed to the upper trinocular input of an optical microscope, passed through a 50% beam splitter to the carousel of objectives with NA = 0.25 (20×) and 0.65 (40×), and were then focused into rings with the characteristic radii (at a 1/e intensity level) of 4.2–4.5 and 1.1–1.4 μm [see formulas (1) and (2)] on the gold film accommodated on a motorised stage for 3D nanopositioning. In the nanotexturing regime ($\mathcal{E}$ = 0.08–2 μJ), after each pulse this substrate was translocated for obtaining linear structures of microopenings or their square arrays at different pulse energies (Fig. 3). The microtextured film surfaces were investigated with an Altami-6 optical microscope and a JEOL 7001F scanning electron microscope (SEM).

Figure 3 shows two series of separate structured ring-shaped microholes with gold nanodiscs persisting at their centres. The microholes were made by the single pulses of laser radiation in the form of Laguerre–Gaussian beams for NA = 0.25, 0.65 and different energies. Like under Gaussian beam irradiation, increasing the energy of a laser pulse resulted in a gradual increase in the outer radius R_h of these holes, while their inner radius (the radius of the disc) r_h, as would be expected, shortened with increasing $\mathcal{E}$. In this case, the value of w_0 (the circumference radius at which the energy density F is highest) may be calculated from Eqn (1) [3]. The asymptotic w_0 values corresponding to the approach to w_0 from the sides of the outer (w_1) and inner (w_2) radii were expressed with the inclusion of only the exponential factor for the outer radius R_h and the preexponential factor for the inner radius r_h [see formulas (2)]:

$$F(r) = \mathcal{E}\frac{r^2}{\pi w_0^4}\exp\left(-\frac{r^2}{w_0^2}\right), \quad (1)$$

$$F(R_h) \propto \exp\left(-\frac{R_h^2}{w_1^2}\right), \quad F(r_h) \approx \mathcal{E}\frac{r_h^2}{\pi w_2^4}. \quad (2)$$

In our experiments w_1 = 4.5 ± 0.3 μm (w_2 = 4.2 ± 0.4 μm) for a nanotexturing threshold $F \approx 0.7$ J cm^{-2} for NA = 0.25 and w_1 = 1.4 ± 0.1 μm (w_2 = 1.1 ± 0.1 μm) for a threshold $F \approx 2$ J cm^{-2} for NA = 0.65 (Fig. 3). As is well known, with the use of different numerical apertures the nanotexturing thresholds also differ due to different electron dynamics in gold on a subpicosecond time scale [13], which depends on the laser energy density. As is noteworthy, for the weaker focusing (NA = 0.25) with $w_{1,2} \geqslant 4$ μm, in the surface-enhanced analytical spectroscopy there is no interaction of the radiation with the central nanodiscs of diameter ~1 μm, while in the case of stronger focusing (NA = 0.65) the interaction is rather good: The peak of the ring-shaped energy density distribution overlaps with the disc and hole edges.

The resultant dependences of microhole dimensions on the energy of laser pulses were used for making several arrays of microholes with different outer and inner diameters (Fig. 3) for the comparative spectral analysis of their size-dependent plasmonic characteristics and the characteristics of the ordinary microholes of similar size produced by Gaussian beams.

In the regime of subablative surface-enhanced analytical spectroscopy with the use of nanostructures, the same but strongly attenuated ($\mathcal{E} \leqslant 0.05$ μJ) Laguerre–Gaussian laser beams enter the upper illumination channel of an MSFU-K microscope-spectrophotometer (LOMO) through a 50% beam splitter and are focused by objectives (NA = 0.25 and 0.65) onto the textured gold film placed on the microscope slide (Figs 1 and 2). A monolayer of rhodamine 6G was deposited by placing a microdroplet of its ethanol solution on the structured surface. The 470–700 nm photoluminescence (PL) spectra were recorded from the monolayer areas ~25 and 13 μm in diameter using an aperture stop of diameter 0.5 mm for the microscope objectives with NA = 0.25 (20×) and 0.65 (40×). Furthermore, we obtained white-light reflec-

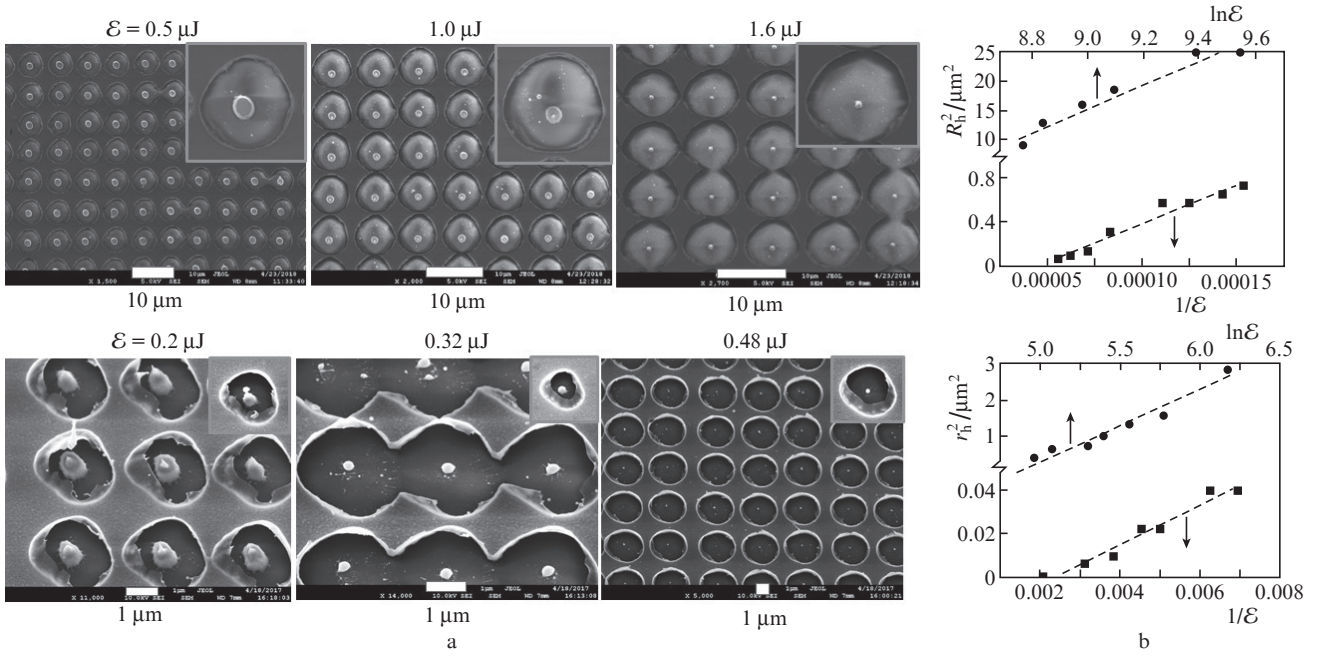

Figure 3. SEM images of structured microhole arrays (the insets: individual microholes) produced for different $\mathcal{E}$ and NA = 0.25 (upper row) and 0.65 (lower row) (a) as well as squared outer (R_h^2) and inner (r_h^2) hole radii as functions of $\ln\mathcal{E}$ and $1/\mathcal{E}$ ($\mathcal{E}$ in nJ), which permit obtaining the focal beam parameters using the above Eqns (1) and (2) (b).

tion and transmission spectra for the structured and ordinary microholes with the use of their 50-μm wide arrays (5 × 5 elements and 15 × 15 elements for the arrays written for NA=0.25 and 0.65, respectively). These spectra were recorded in a range of 400–900 nm with a microscope-spectrophotometer to reveal their plasmon resonances. In this case, the source of white light (a halogen lamp not shown in Fig. 1) was located under the sample. In comparison with the NA = 0.25 objective, the NA = 0.65 objective provided a larger collection angle and a higher collection efficiency as well as a four-fold increase in photoluminescence yield (Fig. 4), which is in reasonable conformity with the scaling coefficient for collection efficiency proportional to NA^2. This testifies to a reasonable agreement between the microhole size and the diameter of incident structured exciting laser beams for NA equal to 0.25 and 0.65.

To characterise the plasmon properties and the corresponding electric field distributions, we also performed auxiliary numerical simulations involving the finite integration technique (FIT). In our model a linearly polarised plane electromagnetic wave in the air was normally incident on a ring-shaped opening (R_h = 1.5 μm, r_h = 0.5 μm) in a 50-nm thick gold film deposited on a glass substrate of infinite thickness. The model used periodic boundary conditions in the xy plane. The appearance of the three-dimensional sample model is displayed in Fig. 5.

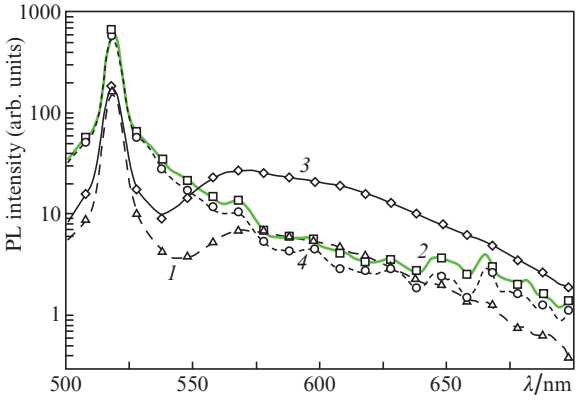

Figure 4. PL spectra of a microhole with (*1*, *3*) and without (*2*, *4*) a rhodamine 6G layer obtained with the use of objectives with NA = (*1*, *2*) 0.25 and (*3*, 4) 0.65. The uneven shape of the spectra in the absence of the dye is, among other reasons, due to the contributions from the angular components of the pump radiation scattered by the microhole.

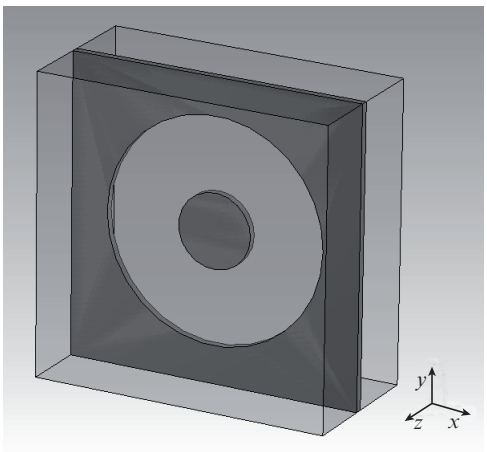

Figure 5. Three-dimensional model of the sample. The electromagnetic wave propagates in the negative z-axis direction.

3. Results and their discussion

3.1. Spectral investigations of structured microholes

Structured microholes resemble a parabolic microantenna with a through hole/crater (a plasmonic mirror, which focuses the near-field radiation [14]) and a central nanodisc – a nanoantenna. As a result, for white light (λ = 400–900 nm) the transmission (Figs 6, 7) and reflection (Figs 8, 9) coefficients for ordinary and structured microholes gradually become respectively higher and lower with increasing the hole size throughout the spectral range. Meanwhile, the transmission spectra of all microholes normalised to the transmission spectrum of the initial gold film with its broad (about 520 nm) plasmon resonance [15] demonstrate an additional peak in a range of 750–850 nm (Fig. 10). Furthermore, in comparison with ordinary microholes the transmission coefficients for the structured microholes of the same size are 4–8 times higher, which is supposedly attributable to the plasmonic enhancement of forward and backward radiation scattering by the central nanodisc antenna in this spectral range.

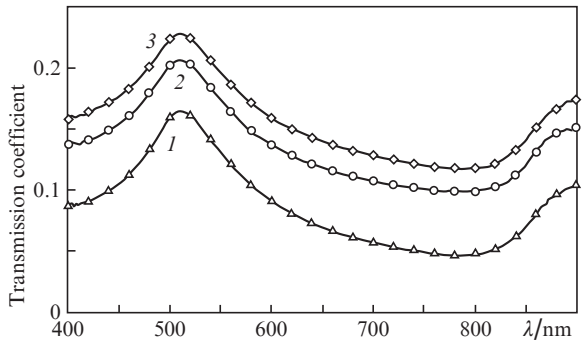

Figure 6. Transmission spectra of ordinary microholes with R_h = (*1*) 2.5, (*2*) 3.5, and (*3*) 4 μm.

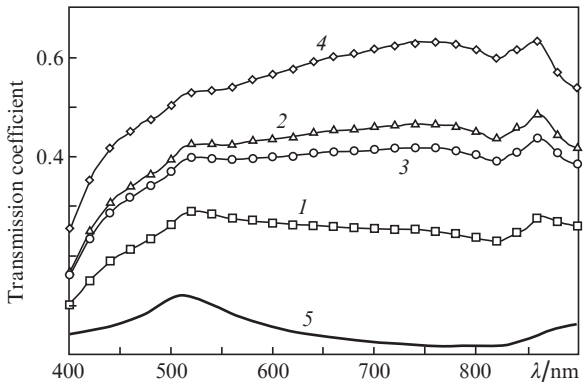

Figure 7. Transmission spectra of the structured microholes with R_h = (*1*) 1.5, (*2*) 2.5, (*3*) 3.5, and (*4*) 4.5 μm as well as of (*5*) a non-structured gold film, in which plasmon resonance may occur.

For characteristic nanostructure dimensions R_h = 1.5 μm and r_h = 0.5 μm, FIT simulations suggest that only standing waves exist in the air layer between the central nanodisc and the microhole edge for λ < 500 nm (the cutoff wavelength of intense interband transitions in gold [16]) and for a linear

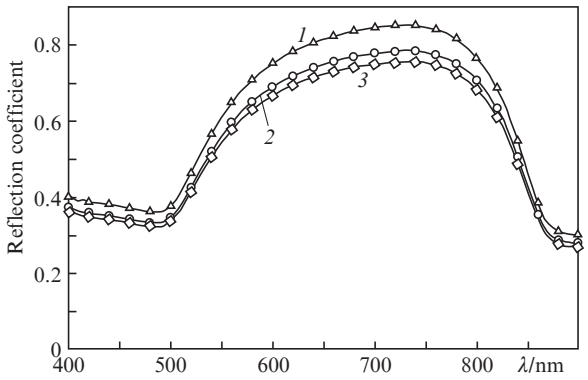

Figure 8. Reflection coefficients of ordinary microholes with R_h = (*1*) 2.5, (*2*) 3.5, and (*3*) 4.5 μm.

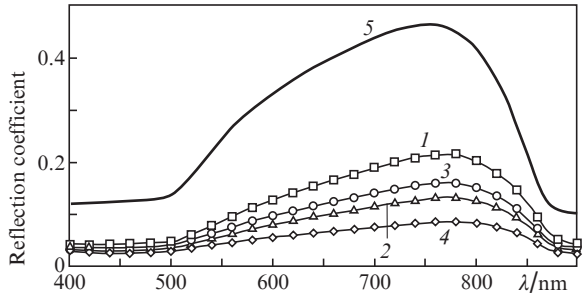

Figure 9. Reflection coefficients of the structured microholes with R_h = (*1*) 1.5, (*2*) 2.5, (*3*) 3.5 and (*4*) 4.5 μm as well as of (*5*) a non-structured gold film.

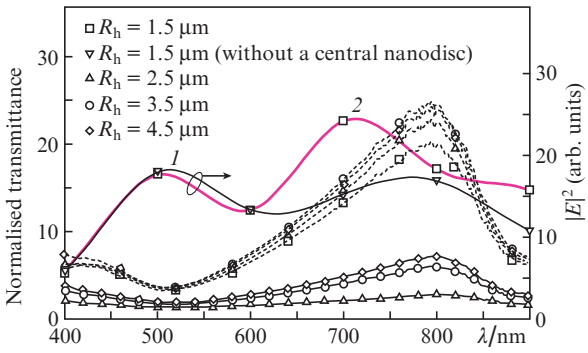

Figure 10. Transmission spectra of the arrays of ordinary holes with R_h = 2.5, 3.5, 4.5 μm and r_h = 0 (solid curves) and structured microholes with R_h = 1.5, 2.5, 3.5, 4.5 μm and r_h = 0.9, 0.85, 0.8, 0.6 μm, respectively, (dashed curves) normalised to the transmission spectrum of a 50-nm thick gold film, as well as calculated squares of the peak near-field amplitudes $|E|^2$ in relation to the wavelength in (*1*) structured and (*2*) ordinary microholes.

light polarisation. The reason is that surface plasmons exhibit a strong attenuation in gold owing to a very high loss in this spectral range. However, gold becomes almost nondissipative in the wavelength domain above 500 nm, and therefore surface plasmons can propagate in a gold film [see peak (*1*) in Fig. 10]. Due to diffraction they interact with the central nanodisc via an air gap to provide a significant enhancement of the electric field at the edges along the hole diameter coinciding with the polarisation direction of laser radiation

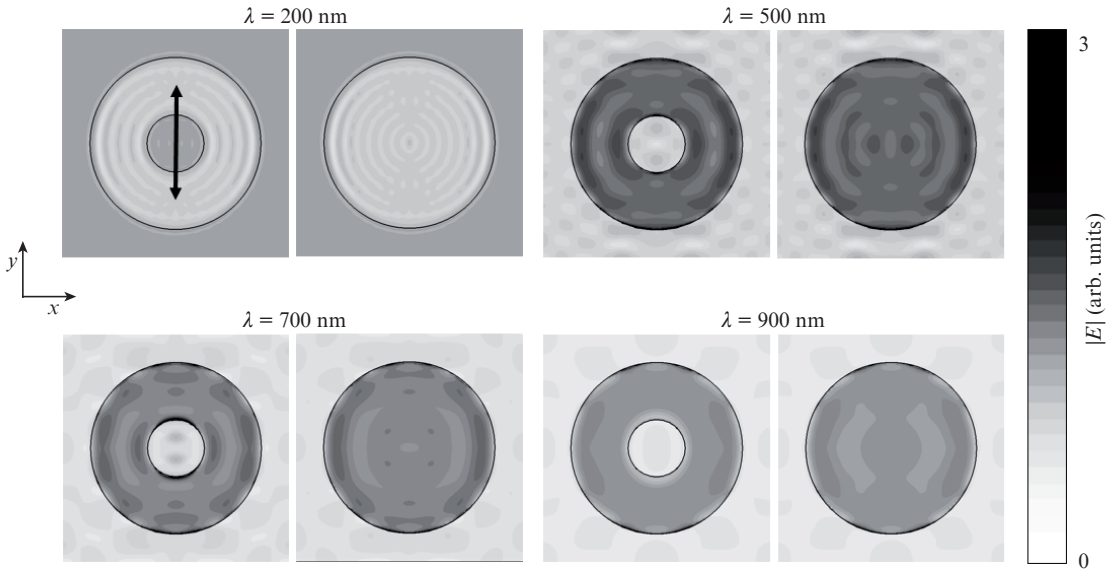

Figure 11. Calculated spatial distributions of the electric field amplitude $|E|$ of a linearly polarised plane wave in the structured hole with R_h = 1.5 μm and r_h = 0.5 μm and in the hole without a central nanodisc at different wavelengths. The arrow indicates the polarisation direction. As is evident from the drawing, for λ = 700 nm the field amplitude increases at the nanodisc edges which are close to the hole diameter parallel to the polarisation direction.

(Fig. 11). This collective mode [see peak (2) in Fig. 10] vanishes when the central nanodisc is absent. At longer wavelengths the optical coupling between the microhole edges and the central nanodisc becomes considerably less efficient [17, 18].

When the electric field distribution in these structures is considered at central sections by *yz* planes, one will see that at certain wavelengths the structure provides the field focusing by the central nanodisc and the appearance of a domain with a high amplitude (Fig. 12).

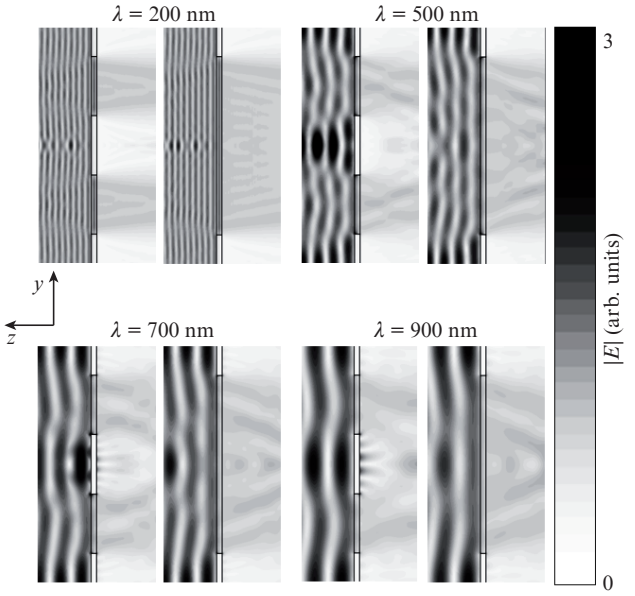

Figure 12. Calculated spatial distributions of electric field amplitude $|E|$ of a linearly polarised plane wave in the structured hole with R_h = 1.5 μm and r_h = 0.5 μm and in the hole without a central nanodisc at different wavelengths (in the *yz* plane). For λ = 500 nm one can see an increase in the field amplitude in the domain above the nanodisc.

3.2. Investigations of surface enhanced dye photoluminescence from structured microholes

For a structured microhole with $R_h \approx 1.5$ μm and $r_h \approx 0.5$ μm, we studied the photoluminescence of a deposited rhodamine 6G monolayer for linear, radial, and azimuthal polarisations of the incident laser radiation in the form of lower-energy Laguerre–Gaussian pulses. With NA = 0.65 objective focusing, all radiation pulses of different polarisation excited separate rhodamine 6G photoluminescence bands peaking at λ = 567–570 nm, which were significantly broadened (by 20–30 nm) and red-shifted by ~10 nm in comparison with the PL band of ethanol dye solution (Fig. 13). This effect may

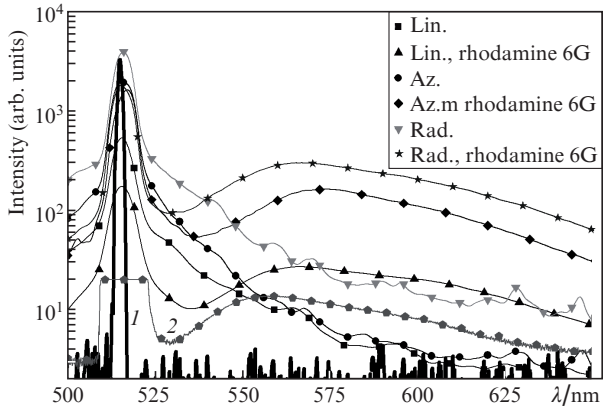

Figure 13. PL spectra of a purely gold structured microhole and the same hole with a rhodamine 6G dye monolayer for linear (Lin.), azimuthal (Az.), and radial (Rad.) polarisations of laser radiation with the use of the NA = 0.65 objective and spectrum of the pump laser radiation (*1*), as well as reference volume PL spectrum of the ethanol rhodamine 6G solution (*2*). The uneven shape of the luminescence spectra without the dye is, among other reasons, due to the contributions from the angular components of the pump radiation scattered by the microhole.

be explained by the interaction of rhodamine 6G molecules with gold nanostructures by charge transfer to the metallic surface [15].

We compared the intensities at the peaks of PL bands in their excitation by the radiation of different polarisation (radial, azimuthal, and linear) for the same incident pulse energy with the use of the NA = 0.65 objection for radiation collection (Fig. 13). The excitation by radially polarised radiation provides a two-fold increase in PL intensity in comparison with the PL intensity under azimuthal excitation and an increase by an order of magnitude (~11) in comparison with the PL intensity excited by linearly polarised radiation. The observed significant PL enhancement may be caused by several physical mechanisms:

1. By the interaction of radially and azimuthally polarised radiation of the visible range with the structured microhole along its entire boundary in contrast to a very narrow sector of the regions of electric field enhancement under linear polarisation (Fig. 11).

2. By the partial transformation of the transverse electric field of the incident radiation to the longitudinal field. This is rather efficient (~31% [9]) when the NA = 0.65 objective is used to focus the radially polarised radiation but is insignificant for the radiation with other polarisation (realised under this transformation is the efficient excitation of localised plasmons in gold nanograins [9]).

3. By the interaction of the incident radiation with λ = 515 nm and the PL with λ = 520–650 nm in the form of a hybridised plasmonic mode 'hole boundary–nanodisc' in the visible and near-IR regions in structured microholes, which has been demonstrated experimentally as well as numerically (see Fig. 11).

4. Conclusions

We have performed direct laser nanotexturing of a gold film and excited the photoluminescence of plasmonic surface structures by vector optical fields with spatially nonuniform polarisation states. This has demonstrated the universal capabilities of lasers to fabricate complicated nanooptical elements, the possibilities for their efficient spectrally, symmetrically, and dimensionally consistent plasmonic excitation as well as for surface-enhanced analytical spectroscopy with the use of nanostructures throughout the visible range. The special features of the transmission and reflection of light by these structures were analysed (the transmission coefficients of structured holes are 5–10 times higher than for ordinary holes). Numerical simulations were employed to obtain an estimate of the enhancement of near-field radiation electric field [up to a 19-fold increase in $|E|^2$ (Fig. 10)]. The photoluminescence efficiency was compared for different polarisations of exciting radiation (with the use of radially polarised radiation the PL intensity was 2 and 11 times higher than with the use of azimuthally and linearly polarised radiation, respectively).

Acknowledgements. This work was supported by the Russian Science Foundation (Project No. 17-12-01258) and, for S.I.Kudryashov, by the Programme for Enhancing the Competitiveness of MEPhI (as regards numerical simulation).

References

1. Litchinitser N.M. *Science*, **337** (6098), 1054 (2012).
2. Toyoda K., Takahashi F., Takizawa S., Tokizane Y., Miyamoto K., Morita R., Omatsu T. *Phys. Rev. Lett*., **110**, 143603 (2013).
3. Nivas J.J., He S., Rubano A., Vecchione A., Paparo D., Marrucci L., Bruzzese R., Amoruso S. *Sci. Rep*., **5**, 17929 (2015).
4. Rubinsztein-Dunlop H., Forbes A., Berry M.V., Dennis M.R., Andrews D.L., Mansuripur M., Denz C., Alpmann C., Banzer P., Bauer T., Karimi E., Marrucci L., Padgett M., Ritsch-Marte M., Litchinitser N.M., Bigelow N.P., Rosales-Guzmán C., Belmonte A., Torres J.P., Neely T.W., Baker M., Gordon R., Stilgoe A.B., Romero J., White A.G., Fickler R., Willner A.E., Xie G., McMorran B., Weiner A.M. *J. Opt*., **19**, 013001 (2016).
5. Kuchmizhak A.A., Porfirev A.P., Syubaev S.A., Danilov P.A., Ionin A.A., Vitrik O.B., Kulchin Yu.N., Khonina S.N., Kudryashov S.I. *Opt. Lett*., **42**, 2838 (2017).
6. Syubaev S., Porfirev A., Zhizchenko A., Vitrik O., Kudryashov S., Fomchenkov S., et al. *Opt. Lett*., **42**, 5022 (2017).
7. Melik-Gaykazyan E.V., Kruk S.S., Camacho-Morales R., Xu L., Rahmani M., Zangeneh Kamali K., Lamprianidis A., Miroshnichenko A.E., Fedyanin A.A., Neshev D.N., Kivshar Y.S. *ACS Phot*., **5**, 728 (2017).
8. Raybould T., Fedotov V.A., Papasimakis N., Youngs I., Zheludev N.I. *Appl. Phys. Lett*., **111**, 081104 (2017).
9. Danilov P.A., Saraeva I.N., Kudryashov S.I., Porfir'ev A.P., Kuchmizhak A.A., Zhizhchenko A.Yu., Rudenko A.A., Umanskaya S.F., Zayarnyi D.A., Ionin A.A., Khonina S.N. *JETP Lett*., **107**, 15 (2018) [*Pis'ma Zh. Eksp. Teor. Fiz*., **107**, 18 (2018)].
10. Salter P.S., Booth M.J. *Opt. Lett*., **36**, 2302 (2011).
11. Hasegawa S., Ito H., Toyoda H., Hayasaki Y. *Opt. Express*, **24**, 18513 (2016).
12. Skoulas E., Manousaki A., Fotakis C., Stratakis E. *Sci. Rep*., **7**, 45114 (2017).
13. Danilov P.A., Drozdova E.A., Ionin A.A., Kudryashov S.I., Odinokov S.B., Rudenko A.A., Yurovskih V.I., Zayarny D.A. *Appl. Phys. A*, **117**, 981 (2014).
14. Gubko M.A., Husinsky W., Ionin A.A., Kudryashov S.I., Makarov S.V., Nathala C., Rudenko A.A., Seleznev L.V., Sinitsyn D.V., Treshin I.V. *Laser Phys. Lett*., **11**, 065301 (2014).
15. Maier S.A. *Plasmonics: Fundamentals and Applications* (Berlin: Springer Science & Business Media, 2007).
16. Palik E.D. *Handbook of Optical Constants of Solids* (Orlando: Academic, 1985).
17. Ebbesen T.W., Lezec H.J., Ghaemi H.F., Thio T., Wolff P.A. *Nature*, **391** (6668), 667 (1998).
18. Liu H., Lalanne P. *Nature*, **452** (7188), 728 (2008).